Measurement of the Earth's Gravity Gradient with an Atom Interferometer-Based Gravity Gradiometer

M. J. Snadden, J. M. McGuirk, P. Bouyer,* K. G. Haritos,† and M. A. Kasevich
Physics Department, Yale University, New Haven, Connecticut 06520
(Received 22 January 1998)

We report the demonstration of an atom interferometer-based gravity gradiometer. The gradiometer uses stimulated two-photon Raman transitions to measure the relative accelerations of two ensembles of laser cooled atoms. We have used this instrument to measure the gradient of the Earth's gravitational field. [S0031-9007(98)06679-4]

PACS numbers: 39.20.+q, 03.75.Dg, 04.80.–y, 32.80.Pj

Measurement of the gradient of gravitational fields has important scientific and technical applications. These applications range from measurement of G, the gravitational constant, and tests of general relativity [1,2] to covert navigation, underground structure detection, oil-well logging, and geodesy [3]. This Letter describes the development of a gravity gradiometer whose operation is based on recently developed atom interference and laser manipulation techniques. A crucial aspect of our design is its intrinsic immunity to spurious accelerations.

Our method is illustrated in Fig. 1. We use light pulse atom interferometer techniques [4–6] to measure the simultaneous acceleration of two laser cooled ensembles of atoms. The relative acceleration of the atom clouds is measured by driving Doppler-sensitive stimulated two-photon Raman transitions [7] between atomic ground-state hyperfine levels. Our geometry is chosen so that the measurement axis passes through both laser cooled ensembles. Since the acceleration measurements are made simultaneously at both positions, many systematic measurement errors, including platform vibration, cancel as a common mode.

This instrument is fundamentally different from current state-of-the-art instruments [8,9]. First, the proof masses used in our work are individual atoms rather than precisely machined macroscopic objects. This reduces systematic effects associated with the material properties of macroscopic objects. Second, the calibration for the two accelerometers is referenced to the wavelength of a single pair of frequency-stabilized laser beams, and is identical for both accelerometers. This provides long term accuracy. Finally, large separations ($\gg 1$ m) between accelerometers are possible. This allows for development of high sensitivity instruments.

Our design also differs significantly from that of previously proposed atom interference-based instruments [10]. The "figure-eight" geometry of prior proposals essentially implements two sequential acceleration measurements with a single ensemble of atoms. Consequently, it exhibits poor immunity to platform vibrations. In contrast, our instrument is based on simultaneous acceleration measurements.

Each acceleration measurement uses a $\pi/2 - \pi - \pi/2$ pulse sequence of stimulated Raman laser pulses. This method is described in detail in Refs. [4,5]. Here we briefly summarize the essential ideas. The two-photon Raman pulses drive Rabi oscillations between two atomic ground-state hyperfine levels (for our experiment, the Cs $F = 3$, $m_f = 0$ and $F = 4$, $m_f = 0$ $6S_{1/2}$ ground states) via nearly resonant optical levels (the $6P_{3/2}$ states). The three pulse sequence results in an atom interferometer if the propagation axes for each of the two Raman laser beams counterpropagate. In the limit of short, intense Raman pulses, atoms initially prepared in the $F = 3$ state have probability $P = [1 - \cos\Delta\phi(\mathbf{r})]/2$ of making the transition to the $F = 4$ state following the excitation sequence. For atoms accelerating at a rate $\mathbf{g}(\mathbf{r})$, $\Delta\phi(\mathbf{r}) = (\mathbf{k}_1 - \mathbf{k}_2) \cdot \mathbf{g}(\mathbf{r})T^2$, where T is the time between successive pulses, and $\mathbf{k}_1$ and $\mathbf{k}_2$ are the propagation vectors for the Raman beams of frequency ω_1 and ω_2. By measuring the ground-state populations following the sequence we are able to determine $\Delta\phi(\mathbf{r})$ and thus the projection of $\mathbf{g}$ along the Raman propagation axes (at position $\mathbf{r}$). In this simplified treatment we have neglected the change in $\mathbf{g}(\mathbf{r})$ experienced by each

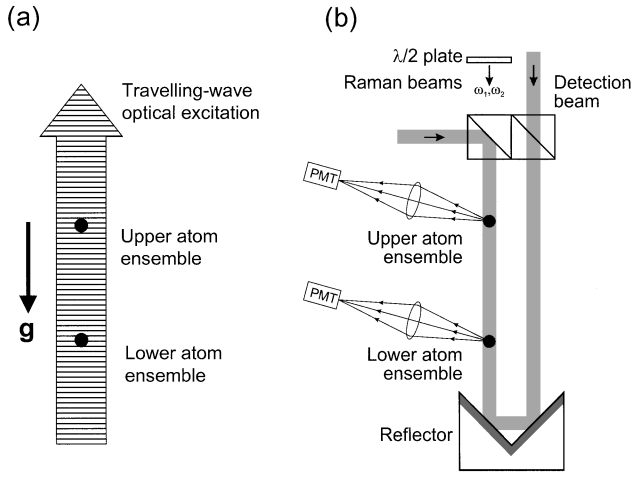

FIG. 1. (a) Schematic illustration of the experiment. (b) Implementation of the optical system.

ensemble over the course of the interferometer pulse sequence [11].

We measure the relative acceleration of the two ensembles along the axis defined by the Raman beams by subtracting the measured phase shifts $\Delta\phi(\mathbf{r}_1)$ and $\Delta\phi(\mathbf{r}_2)$ at each of two locations $\mathbf{r}_1$ and $\mathbf{r}_2$. We extract the gradient by dividing the relative acceleration by the separation of the ensembles. Note that this method determines only one component of the gravity gradient tensor.

In order to see how this scheme is intrinsically immune to platform vibration, we examine the origin of the phase shift $\Delta\phi$ for each interferometer. In the short, intense pulse limit, $\Delta\phi = \phi(t_1) - 2\phi(t_2) + \phi(t_3)$, with $\phi(t) = \int[(\mathbf{k}_1 - \mathbf{k}_2) \cdot \Delta\mathbf{v}(t) - (\omega_1 - \omega_2 - \omega_{\mathrm{hfs}})]\,dt$ [5]. Here $\Delta\mathbf{v}(t)$ is the mean velocity of the atomic wave packet (unperturbed by photon recoil effects) relative to the reference platform at time t; the times t_1, t_2, and t_3 are the times of the $\pi/2$, π, and $\pi/2$ pulses, respectively; and ω_{hfs} is the ground-state hyperfine transition frequency. Vibration of the reference platform will lead to extra phase terms for both the upper and lower interferometers through their influence on the relative velocity $\Delta\mathbf{v}$. However, these terms will be identical for both locations, and will cancel in computation of the phase difference.

The apparatus consisted of two magneto-optical traps [12] separated vertically by $|\mathbf{r}_1 - \mathbf{r}_2| \sim 1.09$ m. Each trap was produced in a separate vacuum chamber. High quality, antireflection coated, optical viewports ($\lambda/10$ p-p over a 3″ diameter substrate) on each chamber allowed the same pair of Raman laser beams to interact with atoms in both chambers. The experiment was run in a pulsed mode, at a repetition rate of 2 Hz. Each shot in principle resulted in a gravitational gradient measurement, and consisted of three sequences: a state-preparation sequence, an interferometer interrogation sequence, and a detection sequence. Each sequence is described in detail below.

The aim of the state-preparation sequence was to produce an ultracold ensemble of atoms in the Cs $F = 3$, $m_f = 0$ hyperfine level. We used the magnetic field insensitive $m_f = 0$ Zeeman sublevel to minimize spurious forces associated with magnetic field gradients. Initially, $\sim 5 \times 10^7$ Cs atoms were captured in each trap from a background Cs vapor pressure of $\sim 3 \times 10^{-9}$ Torr [13]. Following this loading interval, the trapping quadrupole magnetic fields were switched off and the atoms were cooled to ~ 3 μK in polarization gradient optical molasses [14]. The atoms were then optically pumped into the $F = 4$ ground state. Next, a $\sim$300 mG magnetic bias field was pulsed on and a Doppler-sensitive Raman π pulse tuned to be resonant with the $F = 4$, $m_f = 0 \rightarrow F = 3$, $m_f = 0$ transition was applied. The temporal duration of this Raman pulse was chosen to transfer a narrow velocity slice into the $F = 3$, $m_f = 0$ level [7]. This velocity preselection pulse was used to enhance interferometer contrast. After this pulse, atoms remaining in the $F = 4$ manifold were cleared out of the interaction region using momentum transfer from a resonant laser beam. Finally, the magnetic bias field was reduced to $\sim$20 mG. The remaining $F = 3$, $m_f = 0$ population served as the source distribution for the interferometer pulse sequence. We used diode lasers to generate the light needed for the above steps. These lasers were frequency stabilized to atomic resonances using saturated absorption locking techniques.

Following the state-preparation sequence, atoms were subjected to the $\pi/2 - \pi - \pi/2$ interference sequence. We used an all-diode laser system similar to that described in Ref. [15] to drive the Raman transitions, which require two laser beams whose frequency difference is resonant with the Cs 9.2 GHz ground-state hyperfine transition frequency. We generated these beams in the following way. A master laser (SDL 5712 DBR) was both frequency up-shifted and down-shifted with a 4.6 GHz acousto-optic modulator. The two diffracted beams were subsequently amplified using optical injection locking techniques by using each as a seed beam for SDL 5422 laser diodes. The output of each laser then passed through a low frequency acousto-optic modulator ($\sim$40 MHz), with one modulator aligned to produce a frequency up-shift and the other to produce a frequency down-shift. The diffracted beams were overlapped on a polarizing beam-splitting cube, spatially filtered, and then collimated to a 1.7 cm $1/e^2$ diameter. The resulting frequency difference was twice the sum of the low frequency and high frequency modulation sources. A low phase noise HP 8770A arbitrary waveform generator was used as the common source for the low frequency modulators, and provided fine control over the phase and frequency of the Raman difference frequency. We also used these modulators to switch on and off the Raman laser beams.

The pair of collimated Raman beams then copropagated in free space to the apparatus. Copropagating beams minimize potential Doppler shifts of the Raman transition frequency due to vibration of the beam steering optics. The beams were separated using a pair of polarizing beam-splitting cubes just before they entered the vacuum chamber as illustrated in Fig. 1(b). The beam of frequency ω_1 was aligned to pass through both ensembles of atoms, while the other beam of frequency ω_2 was made to propagate parallel to this beam along an axis chosen to miss the atomic clouds. A pair of mirrors mounted just below the exit window of the lower chamber was used to direct the beam of frequency ω_2 along the axis of the downward propagating beam of frequency ω_1. The advantages of this method over the direct retroreflection method used in previous work are that we are able to avoid standing wave excitation of atoms which are nearly at rest and that we minimize ac Stark shifts and residual spontaneous emission due to nonessential beams.

The Raman excitation parameters were chosen with the aim of minimizing unwanted ac Stark shifts and spontaneous emission due to single photon coupling with

the optical transitions, while maintaining an effective two-photon Rabi frequency large enough to excite a significant fraction of the Doppler broadened atomic sources. We typically obtained two-photon Rabi frequencies of $\sim$20 kHz operating at a detuning of $\sim$4.6 GHz from the optical transition. We used a 2.3:1 intensity ratio between the two Raman beams to minimize ac Stark shifts [16].

Over the three pulse sequence the Doppler shift of the Raman resonance induced by the gravitational acceleration was $\sim$1 MHz, while the two-photon Rabi frequency was only $\sim$20 kHz. In order to maintain the resonance condition we phase-continuously chirped the Raman frequency to compensate for this gravitationally induced detuning. We accomplished this by loading the appropriate waveforms into the arbitrary waveform generator.

We detected the number of atoms making the transition to the $F = 4$, $m_f = 0$ level with resonance fluorescence. A counterpropagating pair of beams was aligned along the vertical Raman beam axis and was tuned to excite the $6S_{1/2}$, $F = 4 \rightarrow 6P_{3/2}$, $F = 5$ cycling transition. These beams were pulsed on just after the Raman excitation sequence. The $F = 4$, $m_f = 0$ population was inferred from the scattered light during this detection interval. Since the same beams were used for detection at both locations, noise due to amplitude and frequency fluctuation of these beams was common to both signals.

Characteristic interference data are shown in Fig. 2. We electronically scanned the interference fringes by adding a phase offset to the waveform for the final $\pi/2$-pulse. A uniform background (due to light scattered from background Cs atoms) approximately 10 times larger than the peak-to-peak interference signal has been suppressed. The presence of a gravitational gradient is manifested in a 45 mrad phase shift between the two traces.

In order to suppress further possible systematic phase shifts we also took data with the effective Raman propagation vector reversed. The idea is that reversing the direction of the effective propagation vector will reverse the sign of the gravitational gradient induced phase shift while leaving unchanged the sign and magnitude of possible systematic shifts which are independent of the propagation directions of these beams. Such shifts arise, for example, from time varying magnetic fields (induced by eddy currents associated with the bias field switching used for state preparation) and ac Stark shifts (due to slight mismatches in the spatial modes of the two Raman beams).

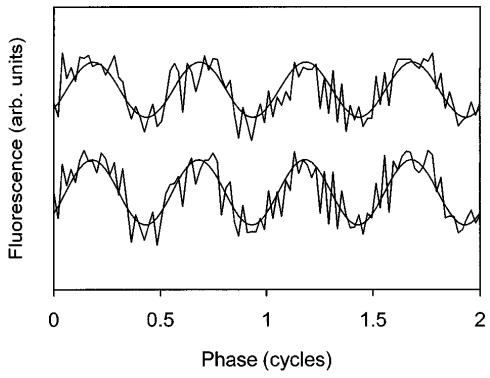

FIG. 2. Typical interference fringes for $T = 30$ msec between each of the Raman pulses. The upper trace is data collected from the upper chamber and the lower trace is data collected from the lower chamber.

In analyzing these data, we were faced with the challenge of extracting the relative phase between two signals with correlated amplitude and phase noise, in the presence of uncorrelated amplitude noise. Before discussing our approach, we will first detail the noise contributions. The dominant source of correlated phase noise was the vibration of the retroreflecting mirror assembly [shown in Fig. 1(b)]. This assembly was rigidly attached to a pneumatically isolated optical table (Newport Research Series with XLA isolators). For the $T = 30$ msec interrogation time data shown in Fig. 2, we estimate the phase noise to be $\sim$400 mrad rms. Sources of correlated amplitude noise included fluctuations in the intensity and frequency of the detection light, as well as the initial number of trapped atoms (the same laser was used for both traps), and were at the 1% rms level (percentage is referenced to the peak-to-peak interference signal level). Uncorrelated noise sources included shot noise due to photons scattered from background Cs atoms during the detection pulse (5% rms) and shot noise due to the number of atoms contributing to the interference signal (6% rms).

We tested several algorithms using simulated data sets. We found that the efficacy of a particular algorithm was strongly dependent on correlated and uncorrelated noise levels. For the noise levels of Fig. 2, the most effective method of determining the relative phase was the subtraction of the phase values extracted from nonlinear curve fits of sinusoids to each data set. In this case, the noise correlation is manifested in a reduced variance for the phase difference as compared with the individual phase variances for the upper and lower data sets. We observed a factor of 2 reduction in the relative phase variance over the estimated variance for completely uncorrelated signals, in good agreement with our simulations. These results were limited by uncorrelated amplitude noise, which we believe can be reduced in future work.

To test the system we have investigated the Earth's gravitational gradient by measuring the phase difference between the two chambers as a function of the time between the interferometer pulses T, as illustrated in Fig. 3. Each data point corresponds to an average of 4×10^4 shots. We used the beam reversal technique described above to suppress a systematic offset of $\sim$10 mrad. A least-squares fit to the expected quadratic dependence of the measured phase difference on T yields a value for the gravity gradient of 3370 ± 175 E ($1\ \mathrm{E} = 10^{-9}\ \mathrm{sec}^{-2}$). The measured gradient value is consistent with the expected value of 3080 E (estimated assuming an inverse square law scaling for $\mathbf{g}$).

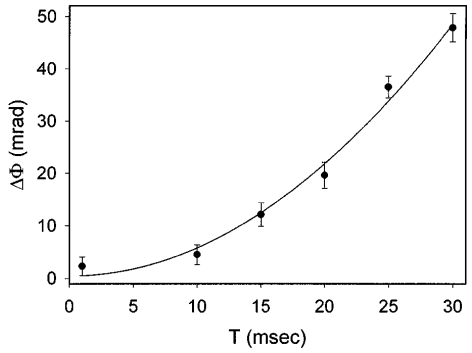

FIG. 3. Measurement of the gravitational gradient of the Earth. The solid line is a least-squares fit to the data.

Significant sources of systematic error include time varying magnetic fields, ac Stark shifts, and platform rotations. We estimate contributions arising from magnetic fields and ac Stark shifts to be below the 10 E level. There are two contributions due to rotations: a Coriolis term and a centrifugal term. The centrifugal term, proportional to Ω^2, is at the 1 E level for $\Omega = \Omega_e$ (the Earth's rotation rate). The Coriolis contribution is proportional to $\Delta\mathbf{v} \times \Omega$, where $\Delta\mathbf{v}$ is the difference of the mean initial velocities of atoms in the upper and lower chambers, respectively. We estimate $|\Delta\mathbf{v}|$ to be no worse than 1 mm/sec, putting an upper limit of 100 E on this contribution for $\Omega = \Omega_e$.

In future work we will explore performance for longer interrogation times and higher momentum transfer atomic beam splitters. For example, working with 200 msec interrogation times, a signal-to-noise ratio of 1000:1 and a $6\hbar\mathbf{k}$ beam splitter should produce a device with a 1 E/Hz$^{1/2}$ sensitivity. In comparison, the state of the art for mobile gravity gradient sensors achieves sensitivities of $\sim$30 E/Hz$^{1/2}$ on noisy platforms [8]. Prototype mobile superconducting sensors have demonstrated sensitivities of $\sim$1 E/Hz$^{1/2}$, but suffer from $1/f$ noise at low frequencies [17]. For some applications, larger physical separations between the accelerometers are possible. In these cases sensitivity scales inversely with accelerometer separation.

Our method can be generalized to measurement of higher order curvature of the gravitational field. For example, a $\pi/2 - \pi - \pi - \pi/2$ sequence could be used to measure the second order curvature of the gravitational field. This would allow massive, distant objects to be distinguished from lighter, local objects.

In conclusion, we have developed an atom interferometer-based gravity gradiometer. With this device we have measured the gradient of the Earth's gravitational field, and demonstrated its immunity to spurious vibrations. The performance of future devices is likely to exceed that of the present state of the art.

This work was supported by the ONR. We thank Matt Thompson for his technical assistance.

*Present address: Groupe d'Optique Atomique, Institut d'Optique Théorique et Appliqué, BP 147, 91403 Orsay, France.

†Present address: Hewlett-Packard Laboratories, 3500 Deer Creek Road, Palo Alto, CA 94304.

[1] B. Mashhoon and D. Theiss, Phys. Rev. Lett. **49**, 1542 (1982).
[2] B. Mashhoon, H. Paik, and C. Will, Phys. Rev. D **39**, 2285 (1989).
[3] N. Sneeuw, R. Rummel, and J. Müller, Class. Quantum Grav. **58**, A113 (1996).
[4] B. Young, M. Kasevich, and S. Chu, in *Atom Interferometry*, edited by P. Berman (Academic Press, New York, 1997).
[5] M. Kasevich and S. Chu, Appl. Phys. B **54**, 321 (1992).
[6] M. Kasevich and S. Chu, Phys. Rev. Lett. **67**, 181 (1991).
[7] M. Kasevich *et al.*, Phys. Rev. Lett. **66**, 2297 (1991).
[8] C. Jekeli, Geophysics **58**, 508 (1993).
[9] M. Moody and H. Paik, Phys. Rev. Lett. **70**, 1195 (1993).
[10] J. Clauser, Physica (Amsterdam) **151B**, 262 (1988).
[11] Inclusion of this dependence leads to second order corrections to the inferred gradient value. For our measurements, these corrections would be at the 10^{-2} E level, well below our present measurement precision.
[12] E. Raab *et al.*, Phys. Rev. Lett. **59**, 2631 (1987).
[13] C. Monroe *et al.*, Phys. Rev. Lett. **65**, 1571 (1990).
[14] See, for example, J. Dalibard and C. Cohen-Tannoudji, J. Opt. Sci. Am. B **6**, 2023 (1989); P. Ungar *et al.*, J. Opt. Sci. Am. B **6**, 2058 (1989).
[15] P. Bouyer *et al.*, Opt. Lett. **21**, 1502 (1996).
[16] We experimentally verified this ratio by measuring the phase shift arising from an extra nonresonant Raman pulse inserted between the first $\pi/2$-pulse and the π-pulse. We observed no ac Stark induced phase shift due to the presence of this extra pulse when the ratio was set properly.
[17] F. van Kann, M. Buckingham, C. Edwards, and R. Matthews, Physica (Amsterdam) **194B–196B**, 61 (1994).